

1 **This is the accepted manuscript of the paper**

2

3 **Assessment of neutron-induced activation of irradiated samples in a research reactor**

4 **by**

5

6 **Ildikó Harsányi, András Horváth, Zoltán Kis, Katalin Gméling, Daria Jozwiak-**
7 **Niedzwiedzka, Michal A. Glinicki, László Szentmiklósi,**

8

9 **published in**

10

11 **Nuclear Engineering and Technology, [https://www.sciencedirect.com/journal/nuclear-](https://www.sciencedirect.com/journal/nuclear-engineering-and-technology)**
12 **[engineering-and-technology](https://www.sciencedirect.com/journal/nuclear-engineering-and-technology), in 2022**

13

14 **The published form of the paper is available under a Creative Commons license (CC BY-**
15 **NC-ND 4.0) at**

16

17 **<https://doi.org/10.1016/j.net.2022.11.004>.**

18

19

1 **Assessment of neutron-induced activation of irradiated samples in a research reactor**

2 Ildikó Harsányi¹, András Horváth¹, Zoltán Kis¹, Katalin Gméling¹, Daria Jozwiak-

3 Niedzwiedzka², Michal A. Glinicki², László Szentmiklósi^{1*}

4 ¹Centre for Energy Research, Budapest, Hungary

5 ²Institute of Fundamental Technological Research, Polish Academy of Sciences, Warsaw, Poland

6 *Corresponding author. E-mail: szentmiklosi.laszlo@ek-cer.hu

7 **Abstract**

8 The combination of MCNP6 and the FISPACT codes was used to predict inventories of
9 radioisotopes produced by neutron exposure of a sample in a research reactor. The detailed
10 MCNP6 model of the Budapest Research Reactor and the specific irradiation geometry of the NAA
11 channel was established, while realistic material cards were specified based on concentrations
12 measured by PGAA and NAA, considering the precursor elements of all significant radioisotopes.
13 The energy- and spatial distributions of the neutron field calculated by MCNP6 were transferred
14 to FISPACT, and the resulting activities were validated against those measured using neutron-
15 irradiated small and bulky targets. This approach is general enough to handle different target
16 materials, shapes, and irradiation conditions. A general agreement within 10% has been achieved.
17 Moreover, the method can also be made applicable to predict the activation properties of the near-
18 vessel concrete of existing nuclear installations or assist in the optimal construction of new nuclear
19 power plant units.

20
21 Keywords: MCNP6, Monte Carlo simulations, FISPACT, isotope inventory, radioisotope
22 production, neutron activation analysis, mineral aggregate, radiation shielding concrete

1 **1. Introduction**

2 Research reactors are used for decades as neutron sources to produce radioisotopes for
3 medical and industrial applications [1], to study the elemental composition of samples [2], or the
4 radiation-induced degradation of the mechanical properties [3]. These applications developed their
5 procedures and conventions to account for the observed reaction rates, by describing the properties
6 of the neutron field, as well as the time-integrated fluence during irradiation. In many fields, e.g.
7 radiation damage, or isotope production via a threshold reaction, only neutrons falling into a
8 specific energy range are effective [4], and the others are even disadvantageous, so the use of
9 appropriate neutron filters (e.g. cadmium, boron-carbide [5]) might be necessary.

10 The experimental characterization of the neutron field usually relies on the irradiation of
11 flux monitor foils. In isotope production applications, one may use the sub-cadmium flux and the
12 total flux as probed with a gold foil with or without a Cd cover. In k_0 -neutron activation analysis
13 (NAA) [6], the combination of Au 0.1%-Al (IRMM-530), Zr, and Fe monitor foils are used (bare
14 triple monitor method) [7], while in the radiation damage studies [8], Al, Nb, Co, and other long-
15 lived isotopes are applicable.

16 Nowadays, the non-routine irradiation requests are more abundant and increasingly well-
17 specified (e.g. not a minimum activity, but a target activity is requested, gamma dose-rate and
18 temperature constraints are given). Moreover, the target assemblies may contain exotic isotopes in
19 specific geometries. For these isotopes no hands-on experience at the irradiation facility may exist,
20 several trial-and-error test irradiations might be necessary to select the appropriate irradiation
21 channel and optimize the conditions. Further, the predictions relying on the almost undisturbed
22 neutron field, as determined by activation foils and the related activation equations [9], do not
23 necessarily consider the depression of the neutron field for bulky and/or highly-absorbent target

1 materials, nor the effect of neutron resonance shielding [10]. Therefore, a rigorous assessment of
2 the irradiation conditions, the resulting reaction rates, neutron-induced activities [11], and dose-
3 rate levels have become essential for such irradiation applications. This calls for a generalized
4 computational approach.

5 Coherent handling of the sample activation is possible by employing full-scale Monte
6 Carlo computer simulations of the irradiation facility, where the complex interactions between the
7 target and the impinging particles are all considered, coupled to isotope-inventory calculations via
8 one of the well-established FISPACT [12], CINDER [13], ACTYS [14], or ORIGEN [15] codes
9 [16,17]. These solve the Bateman-Rubinson differential equations numerically and keep track of
10 the time-dependent growth and decay of all relevant radionuclides at any time instances.

11 **2. Experimental**

12 The Budapest Research Reactor (BRR) is a tank-type research reactor with thermal power
13 of 10 MW, moderated and cooled by light water. The reactor core is surrounded by a solid
14 beryllium reflector. The maximum thermal flux in the core is about 2.2×10^{14} n/cm²s. Unlike
15 common reactor types, the BRR has a unique core geometry, where the 190 pieces of 19.75%
16 enriched VVR-M2 type (LEU) fuel elements are arranged in a hexagonal pattern. In addition, the
17 core assembly accommodates 3 safety- (SCRAM), 14 shim- and 1 fine-automatic control rods
18 made of boron carbide and fitted with 40 vertical irradiation channels.

19 In this study, we focused on the characterization of the BRR's No. 17 vertical channel,
20 where the irradiations for instrumental neutron activation analysis take place, and for which a vast
21 amount of historical flux measurements are available. In this channel, one can stack five aluminum
22 irradiation capsules on each other. Each of these can contain up to six hermetically sealed quartz

1 ampoules of six or eight mm in diameter, encapsulating the individual samples to analyze, with
2 typical masses of 125-175 mg each. The whole channel rotates around its vertical axis to
3 compensate for any spatial inhomogeneity of the neutron flux at the actual vertical irradiation
4 levels. In the simulations, therefore, we can reproduce this characteristic by defining six identical
5 samples packed together, for each run and taking their average as the representative result.

6 The specific activities of the irradiated samples were measured using the D4 and D5 low-
7 background gamma spectrometers of the NAA lab [18]. At first, we determined the activities of
8 neutron flux monitor foils and powdered samples irradiated in the No. 17 channel of the reactor.
9 After the validation of the simulation values with the measured activities for these quasi-point
10 sources, the scope was extended to a case of bulky samples. For this purpose, a set of
11 $18 \times 18 \times 80 \text{ mm}^3$ cement mortar bars was used. Mortar bars were prepared with the water to cement
12 ratio of 0.47 and mineral aggregates of the maximum aggregate size of 2 mm. The mineral
13 materials were selected to cover a wide range of mineralogical compositions of rocks that
14 determine the mechanical properties, and are useful for the production of concrete for nuclear
15 power plant structures. The design of cement-based composites was guided by the criteria of
16 concrete performance during long-time plant operation and the activation of concrete constituents
17 to be considered during plant decommissioning [19]. The following rocks and minerals were
18 included: granite, quartzite, limestone, trachybasalt, opal, and flint. Powder specimens were
19 manufactured by grinding virgin rock aggregates and cement mortar bars, down to the size <45
20 μm . The mortar bars, as well as their grounded forms, were finally irradiated in the Budapest
21 Research Reactor. All ingredients were previously analyzed by NAA [18] and PGAA [20] for their
22 elemental mass fractions and this information was used to set up accurate material cards for the
23 MCNP and FISPACT codes. The combined PGAA and NAA measurements provided the

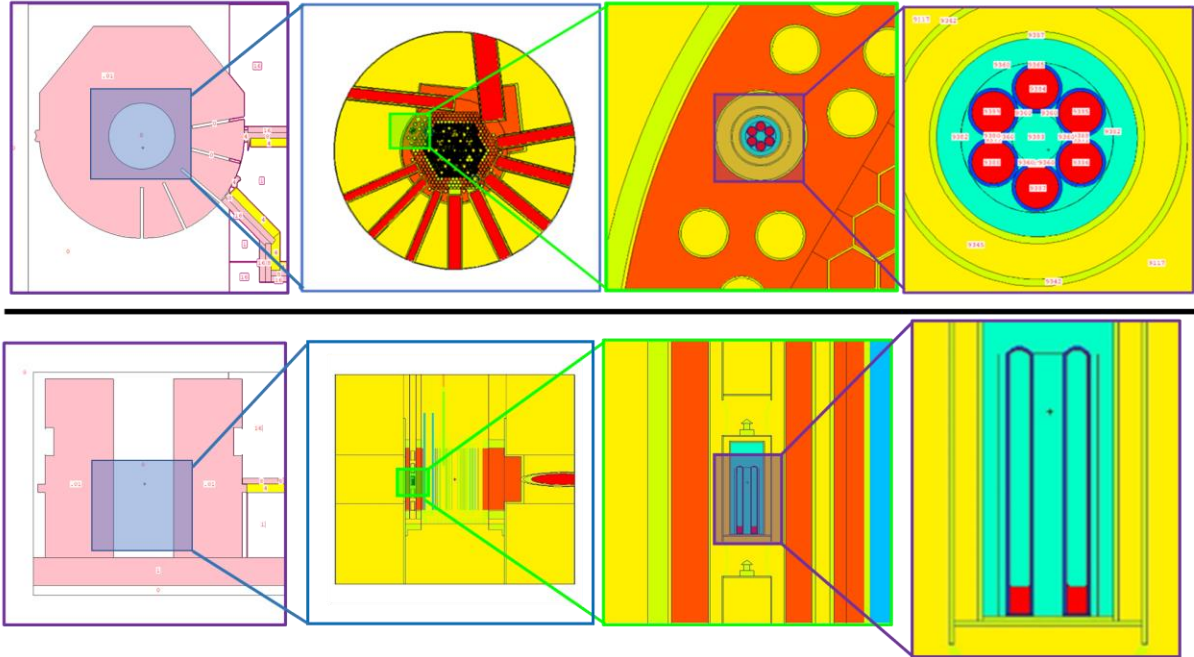
1 concentrations of several low-Z elements (H, B, C, O, Cl), the significant major matrix components
2 (Na, Al, Mg, Si, K, Ca, Fe), as well as many trace components (e.g. Sm, Gd, Co, Cs, Eu Ba, La).
3 By reporting more than 20 trace elements overall, as tabulated in the Electronic Supplementary
4 Information, this composition analysis procedure is more comprehensive than the usual XRF data.
5 This combination of experimentally-obtained concentrations and calculations for the prediction of
6 neutron-induced activation was named NEAAA (*neutron-based elemental composition analysis*
7 *and activity assessment*).

8 **3. Methodology**

9 *3.1. Monte Carlo simulations of the irradiation*

10 Monte Carlo simulations were published for standardized and widespread research reactor
11 types, such as the TRIGA [21,22] and SLOWPOKE [23–25], mostly for reactivity and
12 thermohydraulic calculations, or for decommissioning [26–29]. The use of this technique for
13 irradiation planning, sample activation [30,31], or sample clearance studies is still uncommon.

14 To establish such a tool for the unique core assembly of the Budapest Research Reactor,
15 an MCNP6.2 [32] simulation model of the core was constructed, where the neutron-field
16 properties, such as the integrated intensity, spatial- and energy distributions, could be calculated
17 for any irradiation positions. The geometry of the MCNP model, and that of the irradiation channel
18 No 17, is presented in Figure 1.



1 Reactor biological shielding Reactor vessel Irradiation position No.17 Samples in glass vials

2 *Figure 1. horizontal and vertical cuts of the MCNP reactor model, gradually zooming in to the*
 3 *details of the irradiation position No 17. Materials are color-coded: pink (concrete biological*
 4 *shielding), yellow (cooling water), red (iron structure), orange (beryllium reflector), light-blue*
 5 *(air), dark-blue (silicon sample vial), and purple-red (NAA powder sample).*

6

7 The neutron flux specified by MCNP in the so-called F4 track length estimates per volume
 8 tally (Φ_{F4}) are normalized per source neutron. To get to the real flux intensity, this must be scaled
 9 up using Eq. (1):

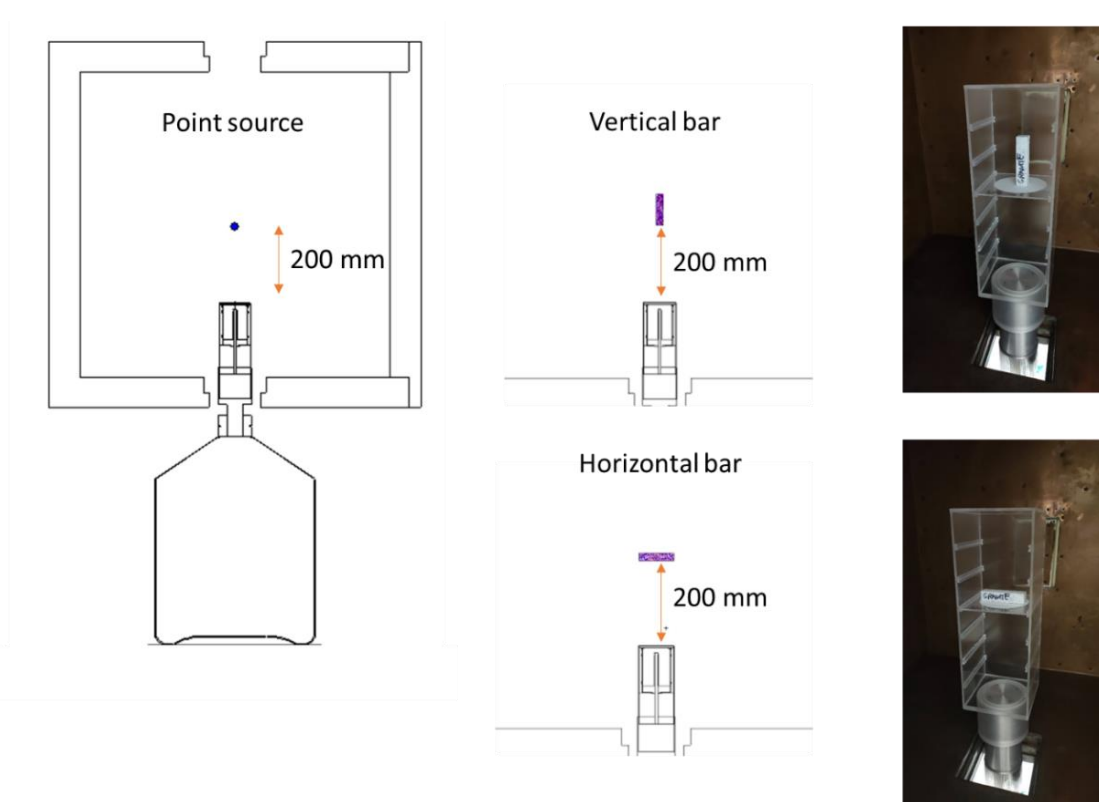
10
$$\Phi = \frac{P \cdot \bar{v}}{1.622 \times 10^{-13} \cdot w_f k_{eff}} \Phi_{F4} = 7.646 \cdot 10^{17} \Phi_{F4} \quad (1)$$

1 where P is the reactor thermal power, $\bar{\nu}$ is the average number of neutrons produced per fission,
2 w_f is the energy released per fission, k_{eff} the calculated reactor multiplication factor, and Φ_{F4} is the
3 flux normalized per source neutron [cm^{-2}] from the MCNP output [33].

4 The case of bulky samples was assessed also by using F4 tallies, where FM cards were set
5 up for the radiative neutron capture reaction (ID 102 from the ENDF library) of each relevant
6 isotope, printing out the volumetric average of the neutron capture rate per isotope of interest in
7 the entire volume of the sample. This simulation was repeated with the identical geometry, but
8 with a target material density reduced by a factor of 1000, representing an infinitely diluted matrix.
9 The ratio of the capture reaction rates with and without dilution, and normalized with the dilution
10 factor, provided the neutron self-shielding correction factor of the voluminous sample. The
11 subsequent isotope inventory calculations are multiplied by this factor to arrive at a well-justified
12 activation estimation for the real sample geometry. For visualization of the flux depression, in
13 some cases, we also used 3D mesh tallies, which provide the spatial distribution of all these
14 quantities.

15 3.2. Monte Carlo simulations of the activity measurement

16 The experimental activities of the irradiated samples were measured using well-calibrated
17 HPGe detectors placed inside a low-level iron counting chamber [18]. To consider the gamma self-
18 absorption and efficiency variation of the bulky samples for the activity measurement, the MCNP
19 model of the gamma spectrometer was also established. We used SuperMC [34] to machine-
20 convert the CAD geometries of the iron counting chamber and the detector (except for the
21 dimensions of the crystal) to MCNP format. Subsequently, the details of the Ge crystal were set
22 up based on the fine-tuned values of the factory-specified dimensions.



1

2 *Figure 2. the MCNP model of the gamma spectrometer to establish the efficiency transfer function*
 3 *of bulky samples*

4 With MCNP, the ratio of the counts in the real geometry and the corresponding point-
 5 source geometry was calculated, and this efficiency transfer function was used to scale the
 6 experimental efficiency curve of the spectrometer (measured using certified sealed point sources).
 7 These activities, being corrected for the geometric effect and the gamma self-absorption, were
 8 used to benchmark FISPACT.

9

10 *3.3. Isotope inventory calculations by FISPACT*

11 Using the neutron field parameters and the composition of the target, a radioisotope
 12 inventory for any time instance can be obtained by using either the MCNP's built-in CINDER

1 routines or in our case, by the FISPACT code. The best coupling was achieved between MCNP
2 and FISPACT when the F4 tally data were tabulated according to the CCFE-709 group energy
3 structure [35], one of the native energy-bin sets of FISPACT, ranging from 10^{-5} eV to 10^9 eV. This
4 way, the inaccuracy related to internal energy-spectrum rebinning could be avoided, which, for
5 instance, created unrealistic discontinuities when feeding in the neutron spectrum according to the
6 UKAEA-1102 tabulation. We used the FISPACT's TENDL-2017 nuclear data library for our
7 calculations.

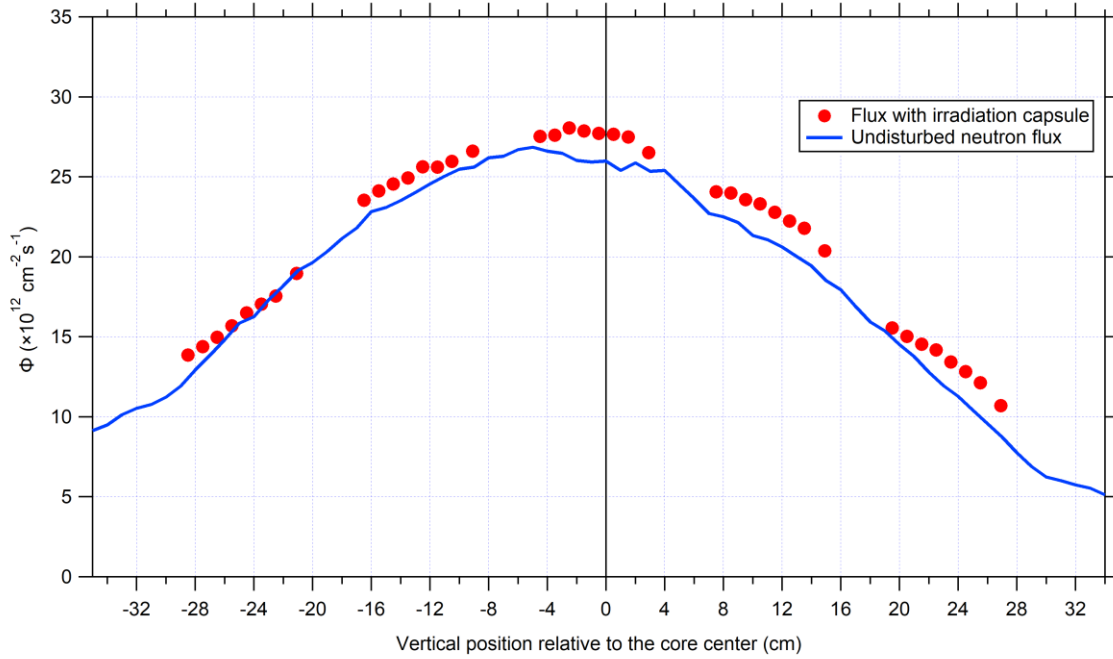
8 These FISPACT activity calculations not only account for the major contributors to gamma
9 dose rate but also for the decays to the ground state, that are without gamma emission, or decays
10 emitting very low-energy gamma radiation that falls below the low-level discriminator of the
11 gamma spectrometer. These are invisible to our NAA experiments but still can contribute to the
12 total activity of the samples.

13

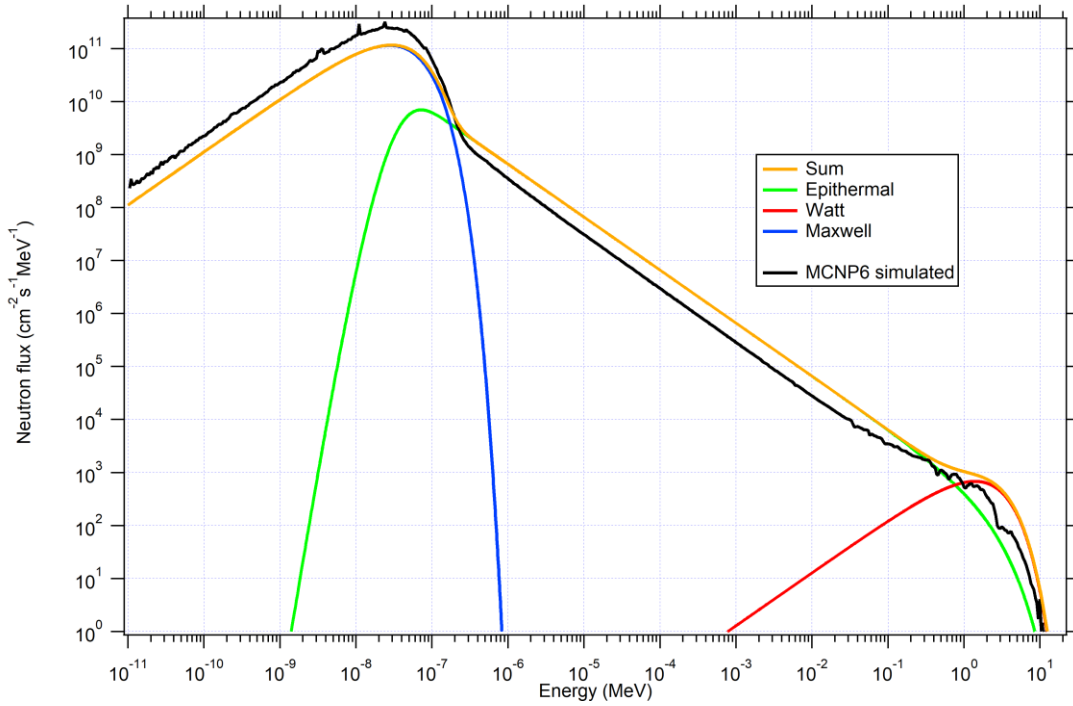
14 **4. Results and discussion**

15 *4.1. Activation of flux monitors*

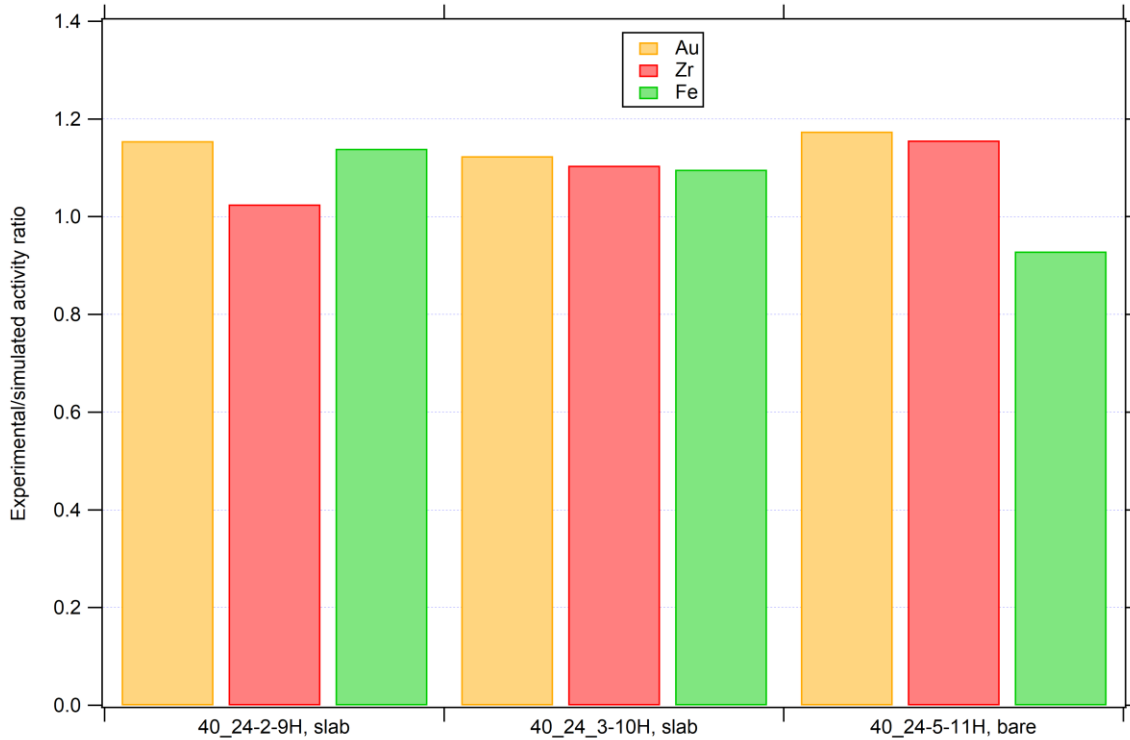
16 After applying the scaling factor of Eq. (1), the MCNP-calculated energy distribution of
17 the neutron fluxes at the five vertical positions of the No. 17 channel is depicted in Figure 3a, while
18 the vertical flux profile along the long axis of the channel is shown in Figure 3b. We can conclude
19 that the energy distributions are similar and differ only in their amplitudes. The absolute flux has
20 its maximum near the center plane of the core and shows a parabolic profile. Note that the presence
21 of the NAA samples and the sample containers have a considerable impact on the magnitude of
22 the neutron flux compared to the undisturbed neutron field.



1
 2 *Figure 3b. the simulated vertical neutron intensity profile in the five positions (1-5 from left to*
 3 *right) of the No. 17 channel.*



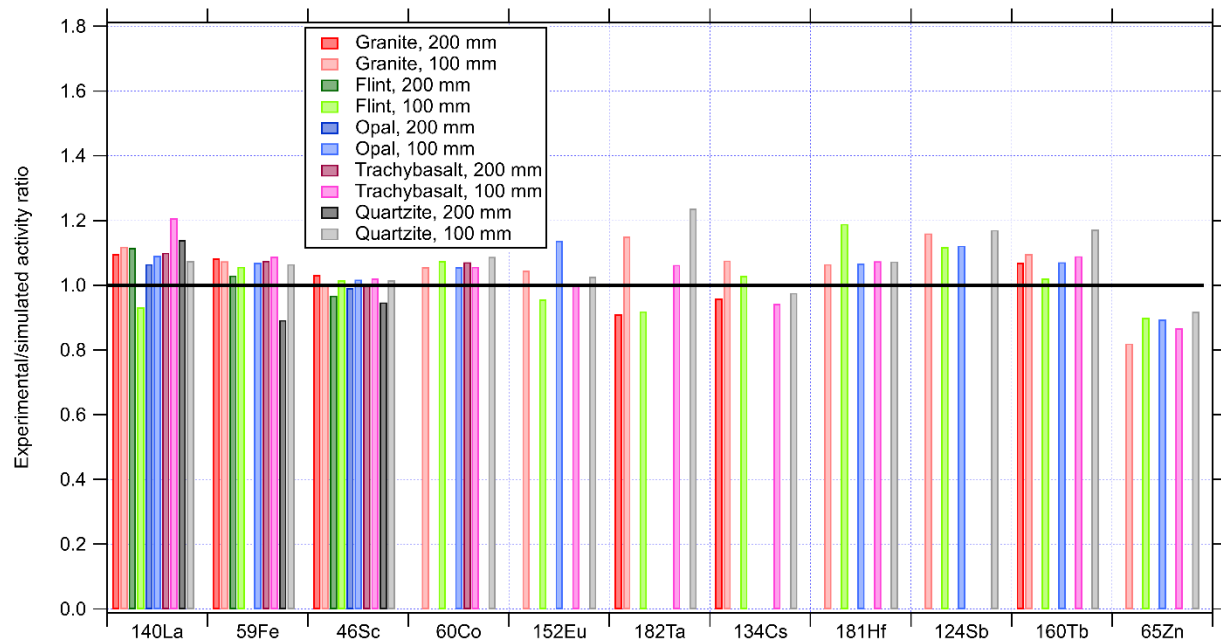
4
 5 *Figure 4a: the measured (orange) vs. calculated (black) flux distributions in Pos. 2 of the No. 17*
 6 *channel*



1
 2 *Figure 4b: the measured over calculated activities of Au 0.1%-Al (IRMM-530), zirconium, and*
 3 *iron foils irradiated in Pos. 2 of the No. 17 channel.*

4 *4.2. Activation of powdered materials*

5 The activation properties of ground mortar samples were also successfully reproduced by the
 6 FISPACT. Here the emphasis was laid on the long-lived radioisotope contents, as they influence
 7 most of the post-irradiation sample clearance issues as well as the decommissioning costs of a
 8 nuclear facility. As shown in Figure 5, we were able to reproduce the measured activation within
 9 about 10%, while the uncertainty margin of the experimental vs simulated ratios was about 5%.
 10 Missing bars mean that the radioisotope was not detected experimentally in the given sample so
 11 the ratio could not be calculated.



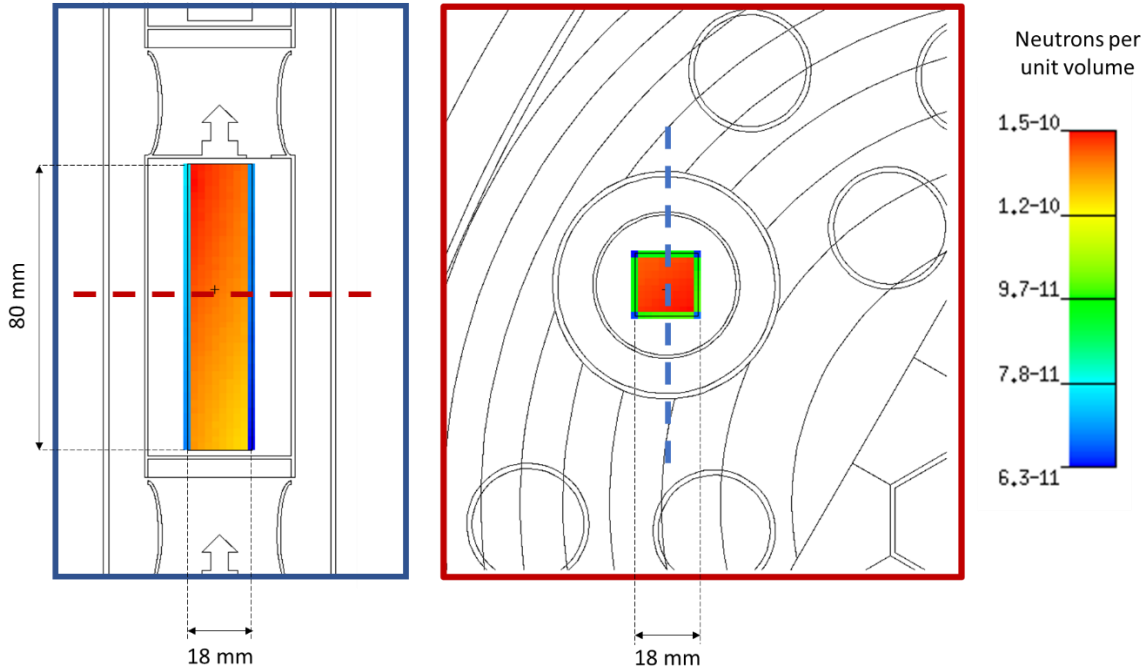
1

2 *Figure 5: the ratios of the measured and predicted activities for the ground mortars loaded with*
 3 *various additives, in a point-source geometry. The first gamma counting has been done at a 200*
 4 *mm sample-to-detector distance, while the second at 100 mm.*

5 *4.3. Activation of bulky mortar samples*

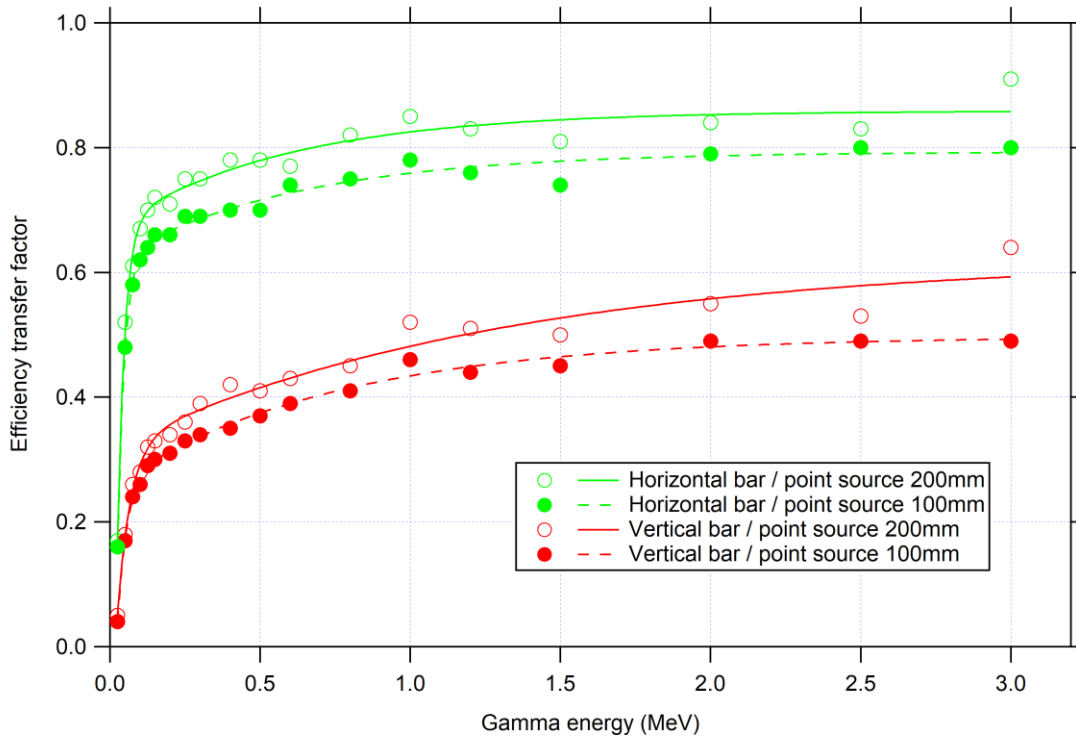
6 In the case of the bar samples, neither the neutron self-shielding nor the gamma self-absorption
 7 was found to be negligible. The former effect is visualized in Figure 6, where a vertical and a
 8 horizontal cut of the 3D simulation mesh are shown, sampling the number of neutrons per unit
 9 volume. There is a gradient of the neutron intensity of about 20% that is fully consistent with the
 10 results of Figure 3b.

11



1

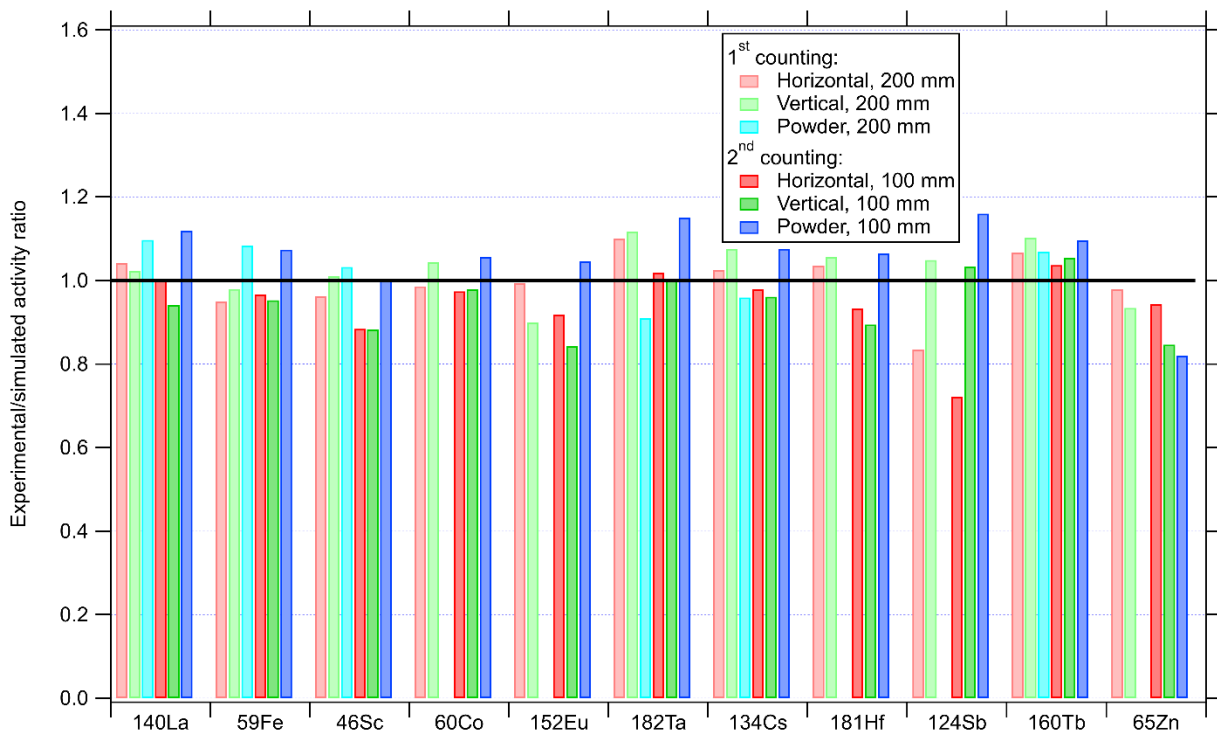
2 *Figure 6: the neutron flux intensity within the granite-loaded mortar test sample from MCNP*
 3 *simulation.*



4

5 *Figure 7: the efficiency-transfer factors between horizontally and vertically placed bulky*
 6 *samples and corresponding point sources*

1 The latter effect, i.e. the combination of gamma self-absorption and the change in the solid angle
 2 during gamma-spectrometry measurements was also simulated, using the detector geometry
 3 shown in Figure 2. The efficiency-transfer functions [37] relative to a point source were obtained
 4 for the horizontal and vertical placements of the bars, for both 100 mm and 200 mm sample-to-
 5 detector distances (Figure 7). When we applied these correction curves, a very good agreement
 6 was achieved between the measured and simulated data for most of the relevant radionuclides, not
 7 only for the powdered case but also for horizontal and vertical solid bar geometries. This is
 8 evidenced in Figure 8.



9
 10 *Figure 8: the experimental activity divided by the simulated activity for the horizontally and*
 11 *vertically placed granite-loaded mortar bars, as well as the corresponding point-like ground*
 12 *sample. The first gamma-measurement took place at 200 mm, 100-150 h after irradiation, while*

1 *the second run at 100 mm, 250-400 h after irradiation. Note that not every radionuclide was*
2 *detectable in all measurements*

3 **5. Conclusions and Outlook**

4 We worked out the NEAAA method, i.e. the combination of i) experimental composition
5 measurement by PGAA and NAA, ii) MCNP-based irradiation calculations, and iii) FISPACT-
6 based radioisotope inventory calculations, to predict the activation of targets placed into a vertical
7 channel of the Budapest Research Reactor. This approach is general enough to handle different
8 target materials, shapes, and irradiation conditions. The calculations were validated with
9 irradiations at the No 17 vertical channel of our reactor at 10 MW power. Flux monitor foils, multi-
10 component powdered NAA samples, and bulky mortar bars were tested, showing increasing
11 complexity, and a decent agreement was achieved in all cases. The ratios of experimental and
12 simulated activities agreed typically within 10%, while the uncertainty margin was about 5%-30%.

13 Within the framework of the V4-Korea RADCON project, a systematic study was conducted,
14 sampling all significant domestic gravel and sand mines of Hungary [38], as well as raw material
15 suppliers of cement and other additives. Based on this comprehensive simulation methodology,
16 raw material dataset, and the mixing design of the concrete, our goal is to predict the activation
17 properties of the near-vessel concrete of existing nuclear installations by computer simulations as
18 well as apply it to the optimal construction of new nuclear power plant units.

19 **Declaration of competing interest**

20 The authors declare that they have no known competing financial interests or personal
21 relationships that could have appeared to influence the work reported in this paper.

22 **Acknowledgment**

1 This work was part of the V4-Korea RADCON Project (No. 127102) and received support from
2 the National Research, Development and Innovation Fund of Hungary, financed under the NN_17
3 funding scheme. We thank the financial contribution of the TOURR project (Euratom research
4 and training programme 2019-2020, grant agreement No. 945269). We also acknowledge the
5 valuable collaboration with Péter Juhász, Dávid Hajdú and Viktória Sugár, Gábor Patriskov,
6 Tamás Bozsó, as well as with the ÉMI Non-profit Llc.

7 **Author Contributions**

8 H.I: Software, Validation (FISPACT), Investigation, Data Curation, Formal analysis (PGAA);
9 A.H, Z.K: Methodology, Software (MCNP); K.G. Investigation, Data Curation, Formal analysis
10 (NAA), D.J.N., M.A.G: Resources (Preparation of mortar bars), Funding acquisition; L.Sz:
11 Conceptualization, Methodology, Validation, Resources, Writing - Original Draft, Visualization,
12 Supervision, Project administration, Funding acquisition

13 **References**

- 14 [1] International Atomic Energy Agency, Applications of Research Reactors,
15 INTERNATIONAL ATOMIC ENERGY AGENCY, Vienna, 2014.
16 <https://www.iaea.org/publications/10491/applications-of-research-reactors>.
- 17 [2] S.J. Parry, Activation Analysis | Neutron Activation, in: *Encycl. Anal. Sci.*, 2019: pp. 15–
18 24. <https://doi.org/https://doi.org/10.1016/B978-0-12-409547-2.14532-9>.
- 19 [3] International Atomic Energy Agency, Research Reactor Application for Materials under
20 High Neutron Fluence, INTERNATIONAL ATOMIC ENERGY AGENCY, Vienna, 2011.
21 [https://www.iaea.org/publications/8452/research-reactor-application-for-materials-under-](https://www.iaea.org/publications/8452/research-reactor-application-for-materials-under-high-neutron-fluence)
22 [high-neutron-fluence](https://www.iaea.org/publications/8452/research-reactor-application-for-materials-under-high-neutron-fluence).
- 23 [4] A.Y. Konobeyev, U. Fischer, S.P. Simakov, Atomic displacement cross-sections for
24 neutron irradiation of materials from Be to Bi calculated using the arc-dpa model, *Nucl.*
25 *Eng. Technol.* 51 (2019) 170–175. <https://doi.org/10.1016/j.net.2018.09.001>.
- 26 [5] R. Szőke, I. Sziklai-László, Epiboron NAA: An option to analyze unfavorable matrices, *J.*
27 *Radioanal. Nucl. Chem.* 275 (2008) 89–95. <https://doi.org/10.1007/s10967-007-6977-6>.
- 28 [6] F. De Corte, *The k0-standardization method*, Rijksuniversiteit Gent, Gent, 1987.

- 1 [7] L. Hamidatou, H. Benkharfia, Experimental and MCNP calculations of neutron flux
2 parameters in irradiation channel at Es-Salam reactor, *J. Radioanal. Nucl. Chem.* 287 (2011)
3 971–975. <https://doi.org/10.1007/s10967-010-0922-9>.
- 4 [8] D. Chiesa, M. Carta, V. Fabrizio, L. Falconi, A. Grossi, M. Nastasi, M. Palomba, S. Pozzi,
5 E. Previtali, P.G. Rancoita, B. Ranghetti, M. Tacconi, Characterization of TRIGA RC-1
6 neutron irradiation facilities for radiation damage testing, *Eur. Phys. J. Plus.* 135 (2020)
7 349. <https://doi.org/10.1140/epjp/s13360-020-00334-7>.
- 8 [9] V.K. Basenko, A.N. Berlizov, I.A. Malyuk, V. V Tryshyn, NAAPRO: A code for predicting
9 results and performance of neutron activation analysis, *J. Radioanal. Nucl. Chem.* 263
10 (2005) 675–681. <https://doi.org/10.1007/s10967-005-0642-8>.
- 11 [10] J. Romero–Barrientos, F. Molina, P. Aguilera, H.F. Arellano, Calculation of self–shielding
12 factor for neutron activation experiments using GEANT4 and MCNP, *AIP Conf. Proc.* 1753
13 (2016) 080018. <https://doi.org/10.1063/1.4955388>.
- 14 [11] M. Blaauw, D. Ridikas, S. Baytelesov, P.S.B. Salas, Y. Chakrova, C. Eun-Ha, R. Dahalan,
15 A.H. Fortunato, R. Jacimovic, A. Kling, L. Muñoz, N.M.A. Mohamed, D. Párkányi, T.
16 Singh, Van Dong Duong, Estimation of ⁹⁹Mo production rates from natural molybdenum
17 in research reactors, *J. Radioanal. Nucl. Chem.* 311 (2017) 409–418.
18 <https://doi.org/10.1007/s10967-016-5036-6>.
- 19 [12] M. Fleming, T. Stainer, M. Gilbert, *The FISPACT-II User Manual*, UK Atomic Energy
20 Authority, Culham Science Centre, Oxfordshire, 2018.
- 21 [13] T.R. England, CINDER – A One-Point Depletion and Fission Product Program WAPD-
22 TM-384, 1962.
- 23 [14] S.C. Tadepalli, P. Kanth, G. Indauliya, I. Saikia, S.P. Deshpande, P.V. Subhash,
24 Development and validation of ACTYS, an activation analysis code, *Ann. Nucl. Energy.*
25 107 (2017) 71–81. <https://doi.org/10.1016/j.anucene.2017.04.016>.
- 26 [15] C. V Parks, Overview of ORIGEN2 and ORIGEN-S: Capabilities and limitations, United
27 States, 1992. http://inis.iaea.org/search/search.aspx?orig_q=RN:23037442.
- 28 [16] D. Hajdú, E. Dian, K. Gméling, E. Klinkby, C.P. Cooper-Jensen, J. Osán, P. Zagyvai,
29 Experimental study of concrete activation compared to MCNP simulations for safety of
30 neutron sources, *Appl. Radiat. Isot.* 171 (2021) 109644.
31 <https://doi.org/10.1016/j.apradiso.2021.109644>.
- 32 [17] D. Hajdú, E. Dian, E. Klinkby, C.P. Cooper-Jensen, J. Osán, P. Zagyvai, Neutron activation
33 properties of PE-B4C-concrete assessed by measurements and simulations, *J. Neutron Res.*
34 21 (2020) 87–94. <https://doi.org/10.3233/JNR-190126>.
- 35 [18] L. Szentmiklósi, D. Párkányi, I. Sziklai-László, Upgrade of the Budapest neutron activation
36 analysis laboratory, *J. Radioanal. Nucl. Chem.* 309 (2016). <https://doi.org/10.1007/s10967-016-4776-7>.
- 37
38 [19] D. Józwiak-Niedźwiedzka, K. Gméling, A. Antolik, K. Dzedzic, M.A. Glinicki,
39 Assessment of Long Lived Isotopes in Alkali-Silica Resistant Concrete Designed for
40 Nuclear Installations, *Materials* (Basel). 14 (2021) 4595.

- 1 <https://doi.org/10.3390/ma14164595>.
- 2 [20] L. Szentmiklosi, T. Belgya, Z. Revay, Z. Kis, Upgrade of the prompt gamma activation
3 analysis and the neutron-induced prompt gamma spectroscopy facilities at the Budapest
4 research reactor, *J. Radioanal. Nucl. Chem.* 286 (2010) 501–505.
- 5 [21] A.D. Loya, S.V. Escamilla, A.M.G. Torres, E.D.V. Gallegos, Verification of a Triga Mark
6 III MCNP model for neutron flux calculations, *Int. J. Nucl. Energy Sci. Technol.* 10 (2016)
7 146. <https://doi.org/10.1504/IJNEST.2016.077480>.
- 8 [22] A. Borio di Tigliole, A. Cammi, D. Chiesa, M. Clemenza, S. Manera, M. Nastasi, L.
9 Pattavina, R. Ponciroli, S. Pozzi, M. Prata, E. Previtali, A. Salvini, M. Sisti, TRIGA reactor
10 absolute neutron flux measurement using activated isotopes, *Prog. Nucl. Energy.* 70 (2014)
11 249–255. <https://doi.org/10.1016/j.pnucene.2013.10.001>.
- 12 [23] F. Puig, H. Dennis, SLOWPOKE-2 alternative core loading configurations analysis for
13 highly improved reactor performance, *Ann. Nucl. Energy.* 128 (2019) 216–230.
14 <https://doi.org/10.1016/j.anucene.2018.12.016>.
- 15 [24] J.C. Rook, K.P. Weber, E.C. Corcoran, Advanced MCNP Simulation of the Neutron and
16 Photon Flux and Absorbed Dose Rates for the SLOWPOKE-2 Nuclear Reactor at the Royal
17 Military College of Canada, *Nucl. Technol.* 206 (2020) 1861–1874.
18 <https://doi.org/10.1080/00295450.2020.1720557>.
- 19 [25] T.S. Nguyen, G.B. Wilkin, J.E. Atfield, Monte Carlo Calculations Applied to SLOWPOKE
20 Full-Reactor Analysis, *AECL Nucl. Rev.* 1 (2012) 43–46.
21 <https://doi.org/10.12943/anr.2012.00017>.
- 22 [26] A. Septilarso, D. Kawasaki, S. Yanagihara, Radioactive waste inventory estimation of a
23 research reactor for decommissioning scenario development, *J. Nucl. Sci. Technol.* 57
24 (2020) 253–262. <https://doi.org/10.1080/00223131.2019.1667923>.
- 25 [27] A. Rätty, P. Kotiluoto, FiR 1 TRIGA Activity Inventories for Decommissioning Planning,
26 *Nucl. Technol.* 194 (2016) 28–38. <https://doi.org/10.13182/NT15-86>.
- 27 [28] B. Volmert, M. Pantelias, R.K. Mutnuru, E. Neukaeter, B. Bitterli, Validation of MCNP
28 NPP Activation Simulations for Decommissioning Studies by Analysis of NPP Neutron
29 Activation Foil Measurement Campaigns, *EPJ Web Conf.* 106 (2016) 05010.
30 <https://doi.org/10.1051/epjconf/201610605010>.
- 31 [29] B. Babcsányi, S. Czifrus, S. Fehér, Methodology and conclusions of activation calculations
32 of WWER-440 type nuclear power plants, *Nucl. Eng. Des.* 284 (2015) 228–237.
33 <https://doi.org/10.1016/j.nucengdes.2014.11.032>.
- 34 [30] S. Kim, M.H. Kim, A Study on MCNPX-CINDER90 System for Activation Analysis, in:
35 *Trans. Korean Nucl. Soc. Autumn Meet., Pyeongchang, Korea, 2014*: pp. 5–8.
- 36 [31] V. Radulović, R. Jaćimović, A. Pungerčič, I. Vavtar, L. Snoj, A. Trkov, Characterization of
37 the neutron spectra in three irradiation channels of the JSI TRIGA reactor using the
38 GRUPINT spectrum adjustment code, *Nucl. Data Sheets.* 167 (2020) 61–75.
39 <https://doi.org/10.1016/j.nds.2020.07.003>.

- 1 [32] T. Goorley, M. James, T. Booth, F. Brown, J. Bull, L.J. Cox, J. Durkee, J. Elson, M. Fensin,
2 R.A. Forster, J. Hendricks, H.G. Hughes, R. Johns, B. Kiedrowski, R. Martz, S. Mashnik,
3 G. McKinney, D. Pelowitz, R. Prael, J. Sweezy, L. Waters, T. Wilcox, T. Zukaitis, Features
4 of MCNP6, *Ann. Nucl. Energy.* 87 (2016) 772–783.
5 <https://doi.org/10.1016/J.ANUCENE.2015.02.020>.
- 6 [33] G. Žerovnik, M. Podvratnik, L. Snoj, On normalization of fluxes and reaction rates in
7 MCNP criticality calculations, *Ann. Nucl. Energy.* 63 (2014) 126–128.
8 <https://doi.org/10.1016/j.anucene.2013.07.045>.
- 9 [34] Y. Wu, J. Song, H. Zheng, G. Sun, L. Hao, P. Long, L. Hu, CAD-based Monte Carlo
10 program for integrated simulation of nuclear system SuperMC, *Ann. Nucl. Energy.* 82
11 (2015) 161–168. <https://doi.org/10.1016/J.ANUCENE.2014.08.058>.
- 12 [35] UKAEA, CCFE-709 group structure, (n.d.). [https://fispact.ukaea.uk/wiki/CCFE-](https://fispact.ukaea.uk/wiki/CCFE-709_group_structure)
13 [709_group_structure](https://fispact.ukaea.uk/wiki/CCFE-709_group_structure).
- 14 [36] R.M.W. Overwater, J.E. Hoogenboom, Accounting for the Thermal Neutron Flux
15 Depression in Voluminous Samples for Instrumental Neutron Activation Analysis, *Nucl.*
16 *Sci. Eng.* 117 (1994) 141–157. <https://doi.org/10.13182/NSE94-A28530>.
- 17 [37] T. Vidmar, B. Vodenik, M. Nečemer, Efficiency transfer between extended sources, *Appl.*
18 *Radiat. Isot.* 68 (2010) 2352–2354. <https://doi.org/10.1016/j.apradiso.2010.05.010>.
- 19 [38] V. Szilágyi, K. Gméling, S. Józsa, I. Harsányi, L. Szentmiklósi, Oligomictic alluvial
20 aggregates: petro-mineralogical and geochemical evaluation of sandy gravel formations on
21 the middle course of the Danube (Hungary), *Bull. Eng. Geol. Environ.* 80 (2021) 5957–
22 5977. <https://doi.org/10.1007/s10064-021-02271-w>.

23